



Coherent dual-frequency signal generation in an optoelectronic oscillator

SHIFENG LIU,[†] CHANGLONG DU,[†] LI YANG, MINGZHEN LIU, ZHENZHOU TANG,[✉] AND SHILONG PAN^{*} 

[†]National Key Laboratory of Microwave Photonics, Nanjing University of Aeronautics and Astronautics, Nanjing 210016, China

[†]These authors contributed equally to this Letter.

*pans@nuaa.edu.cn

Received 3 March 2023; revised 21 April 2023; accepted 25 April 2023; posted 28 April 2023; published 24 May 2023

Coherent dual-frequency microwave signal generation using an optoelectronic oscillator (OEO) is presented and demonstrated. In the proposed OEO, a dual-band bandpass filter (DB-BPF) is utilized to select two oscillation modes. An external signal is injected into the OEO loop with its frequency equaling the frequency interval of the two oscillation modes. Owing to the modulation nonlinearity of the Mach–Zehnder modulator, the two oscillation frequencies interact with the injection frequency. When the phase and gain conditions are satisfied within the loop, injection locking between the two oscillation signals will be established, and their phases will be synchronized. The effect of gain competition in the OEO loop, which leads to single-frequency oscillation, is suppressed. An experiment is carried out, and two frequencies, of 16.083 GHz and 9.998 GHz, are generated at the same time. The phase noise values are -140.1 and -141.0 dBc/Hz @ 10 kHz, respectively. The coherence between the generated signals and sidemode suppression performance are evaluated. © 2023 Optica Publishing Group

<https://doi.org/10.1364/OL.488711>

A dual-frequency local oscillation (LO) signal can be used for the generation of wideband dual-band RF signals [1–4], and its coherence and purity significantly affect the performance of dual-band radar, weather monitoring systems, global positioning systems, and wireless communications [5,6]. Traditionally, coherent dual-frequency LOs can be obtained by selecting two frequency components from an RF comb or using two synchronized frequency synthesizers [3,7]. The coherence between the two generated frequencies can be guaranteed using a high-stable crystal oscillator, but the phase noise (PN) performance of these LOs is usually limited, especially at high frequencies. Owing to the low loss, wide operation bandwidth, and high Q value, photonic techniques offer several effective ways to generate dual-frequency LOs [2,8–15]. Scotti *et al.* [2] and Brandão *et al.* [8] obtain the dual-frequency signal by simply beating different comb lines of an optical comb in a photodetector (PD) and selecting two individual frequencies with the help of narrow-band RF filters. The stable phase relation between the optical frequency lines of the optical comb guarantees the coherence of the generated two frequencies. However, the repetition frequency

of the optical comb is generally fixed, which results in poor frequency tunability. A dual-frequency signal can also be generated using a dual-beam optically injected semiconductor laser [9,10]. Although frequency tunability can be attained by adjusting the injection power, the PN of the generated signal is usually very high, resulting from the intrinsic wavelength drifting of the semiconductor laser. Another way to produce the frequency-tunable and high-performance dual-frequency signal is to exploit the high- Q optoelectronic cavity of an optoelectronic oscillator (OEO), such as introducing parallel filters [11,12], a multi-channel optical notch filter [13], or polarization multiplexing [14,15] in the OEO-based structure. However, the gain competition [16] in the optoelectronic loop makes it hard to maintain the oscillation at two frequencies concurrently. Besides, the coherence of the two signals is poor because there is no phase-locking mechanism between the two frequencies.

In this Letter, we present a novel approach to generating coherent dual-frequency signals in an OEO loop. In the proposed approach, a dual-band bandpass filter (DB-BPF) is inserted to select two oscillation modes, and an RF signal with its frequency identical to the frequency difference of the two oscillation modes is externally injected into the OEO loop. Thanks to the nonlinearity of the electro-optical intensity modulator in the OEO, mutual frequency conversion and energy coupling between the injection signal and the two oscillation modes occur, in which the injection signal serves as the intermediate frequency. The effect of the gain competition in the oscillation loop is suppressed because of the energy coupling, guaranteeing simultaneous oscillation of the two frequencies. By carefully adjusting the loop gain and phase, mutual injection locking would be established, ensuring the phase coherence of the two oscillation modes.

Figure 1(a) depicts the principle of the coherent dual-frequency RF signal generation using an OEO. The oscillating signal is intensively modulated to a continuous light wave from a laser source in a Mach–Zehnder modulator (MZM), generating an intensity-modulated optical signal. The generated optical signal is converted to a photocurrent in a PD after passing through a coil of single-mode fiber (SMF) with low transmission loss. The output photocurrent is then boosted by an electrical amplifier (EA), electrically filtered by a DB-BPF, and re-injected into the MZM with an external RF signal. The DB-BPF has two RF passbands, with the center frequencies denoted ω_1 and

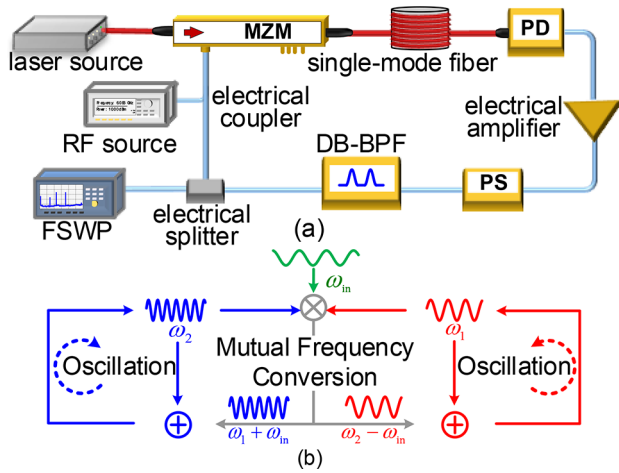


Fig. 1. Principle of coherent dual-frequency signal generation in OEO. (a) Block diagram. (b) Frequency relationships of injection frequency and two oscillation frequencies. DB-BPF, dual-band bandpass filter; FSWP, PN analyzer; MZM, Mach–Zehnder modulator; PD, photodetector; PS, phase shifter; RF, radio frequency.

ω_2 , respectively. The frequency of the injection signal ω_{in} equals $\omega_2 - \omega_1$ in the steady state, and will be blocked by the DB-BPF in the oscillation loop. As depicted in Fig. 1(b), frequency mixing occurs in the MZM, owing to its modulation nonlinearity. During the frequency mixing procedure, the oscillation frequency of ω_2 is downconverted to $\omega_2 - \omega_{in}$ by mixing with ω_{in} . As ω_{in} equals $\omega_2 - \omega_1$ in the steady state, the downconverted frequency equals ω_1 and is injected into the oscillation loop of ω_1 . By carefully adjusting the loop gain and phase, the oscillation loop of ω_1 can be injection-locked by the downconverted signal from ω_2 . At the same time, the oscillation frequency of ω_1 is upconverted to $\omega_1 + \omega_{in}$, and then injection locks the oscillation loop of ω_2 with a similar mechanism. In this way, mutual injection locking between the two oscillation modes is realized, and the loop gain competition is suppressed. Therefore, two stable and coherent frequencies oscillate in the single OEO loop. It should be mentioned that the injection frequency is lower than either frequency of the two oscillation signals, which makes it cost-effective to generate high frequencies with high performance in a single oscillation loop.

Mathematically, the input microwave signal $V_{MZM}(t)$ of the MZM is given by

$$V_{MZM}(t) = V_{in} \cos(\omega_{in}t + \varphi_{in}) + V_1 \cos(\omega_1t + \varphi_1) + V_2 \cos(\omega_2t + \varphi_2) \quad (1)$$

where V_{in} , V_1 , V_2 , φ_{in} , φ_1 , φ_2 are the electrical amplitude and initial phase of the injection signal and the two oscillation signals, respectively. Introducing $V_{MZM}(t)$ to the transmission function of the MZM, the output RF signal of the PD can be written as

$$V_{out}(t) \propto \Re\eta P_c \cos[\gamma_{in} \cos(\omega_{in}t + \varphi_{in}) + \gamma_1 \cos(\omega_1t + \varphi_1) + \gamma_2 \cos(\omega_2t + \varphi_2) + \theta] \quad (2)$$

where \Re is the responsivity of the PD, η is the total loss of the optical link, P_c is the power of the light wave from the laser source, θ is the bias phase, $\gamma_{in} = \pi V_{in}/V_\pi$, $\gamma_1 = \pi V_1/V_\pi$, and $\gamma_2 = \pi V_2/V_\pi$ are the modulation index of the injection signal and the two oscillation signals, and V_π is the RF half-wave voltage of the Mach–Zehnder modulator, respectively. The DC component in Eq. (2) is ignored. In addition, a small-signal modulation

assumption is made in the oscillation loop and the DB-BPF removes high-order harmonics and other inter-modulated frequency components. Thus, the output electrical signal of the DB-BPF can be derived as

$$\begin{aligned} V_{out}(t) \propto & 2\Re\eta P_c \{J_0(\gamma_2)J_0(\gamma_{in})J_1(\gamma_1) \sin(\theta) \cos(\omega_1t + \varphi_1) \\ & + J_0(\gamma_{in})J_0(\gamma_1)J_1(\gamma_2) \sin(\theta) \cos(\omega_2t + \varphi_2) \\ & - J_0(\gamma_2)J_1(\gamma_{in})J_1(\gamma_1) \cos(\theta) \cos[(\omega_1 + \omega_{in})t + \varphi_1 + \varphi_{in}] \\ & - J_0(\gamma_1)J_1(\gamma_{in})J_1(\gamma_2) \cos(\theta) \cos[(\omega_2 - \omega_{in})t + \varphi_2 - \varphi_{in}]\} \end{aligned} \quad (3)$$

where $J_n(*)$ is the n th Bessel function. According to Eq. (3), the MZM should be properly biased to balance the modulation nonlinearity and the loop gain.

As shown in Eq. (3), the output signal is made up of the oscillation frequencies, ω_1 , ω_2 , and their frequency-converted components, $\omega_1 + \omega_{in}$ and $\omega_2 - \omega_{in}$. Here, the frequency-converted components are generated by the nonlinearity of the MZM. When the injection signal of ω_{in} equals the frequency difference of ω_1 and ω_2 , the downconverted frequency of $\omega_2 - \omega_{in}$ will inject in the oscillation loop of ω_1 , leading to the injection locking at ω_1 in the loop. Meanwhile, the oscillation loop of ω_2 will also be injection-locked to the upconverted frequency of $\omega_1 + \omega_{in}$. The frequency conversion and mutual injection locking procedures sustain the dual-frequency oscillation and correlate the phase of the two frequencies. When ω_2 has a greater power than ω_1 , the power of the downconverted frequency component $\omega_2 - \omega_{in}$ also increases, which reinforces the oscillation of ω_1 , and vice versa, resulting in significant suppression of gain competition. If the externally injected signal is turned off, the two oscillation frequencies will suffer from serious gain competition, and only one frequency can survive in the oscillation loop.

A proof-of-concept experiment is performed to verify the theory and identify relevant RF characteristics, according to Fig. 1(a). The essential parameters of the experimental components and instruments are provided. The output optical power of the narrow-linewidth laser source (1782, Emcore) is 18.9 dBm, and its center wavelength is 1550.2 nm. The Mach–Zehnder modulator (FTM7938, Fujitsu) has an RF bandwidth of >23 GHz and a V_π of 5 V. The transmission loss of the 4-km SMF is around 2.2 dB. The high-speed photodiode (GD45220R, CETC 44) has an RF bandwidth of 20 GHz and a 0.8-A/W responsivity. The RF gain of the low-noise electrical amplifier (EA) (TLNA02G18G, Talent Microwave) reaches 30 dB from 2 GHz to 18 GHz. The DB-BPF has two passbands with the center frequencies located at 10 and 16.083 GHz; the 3-dB bandwidth of each passband is 10 MHz and 20 MHz, respectively. In addition, the injection signal is produced by a microwave generator (E8257D, Keysight), and the spectral properties of the generated RF signals in the proposed scheme are analyzed using a PN analyzer (FSWP26, R&S) with a spectrum analysis component.

To demonstrate the feasibility of the dual-frequency generation proposed in Fig. 1, the output frequency spectra of the DB-BPF are monitored through an electrical power splitter. The loop phase and gain conditions [17] for stable oscillation are achieved by adjusting the phase shifter and the transmission loss of the optical link, and the steady-state results of the OEO are shown in Fig. 2. Figure 2(a) exhibits the measured frequency spectrum of the proposed OEO when the injection frequency is turned off. Owing to the gain competition of the free-running oscillation loop, only the 9.998-GHz frequency oscillates. The electrical power of the oscillation signal is 3.9 dBm. When the

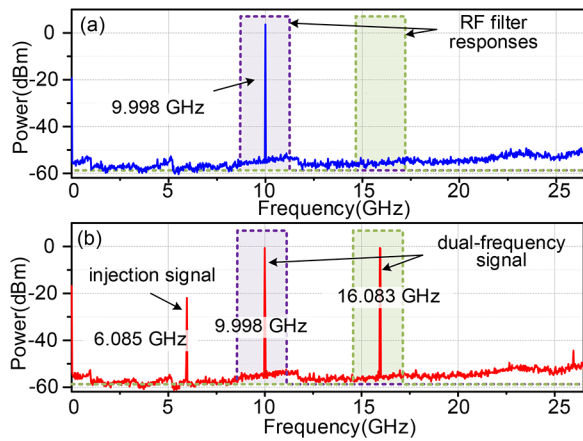


Fig. 2. Output electrical spectra of DB-BPF when injection signal is turned (a) off and (b) on.

injection signal is turned on, two oscillation frequencies are successfully generated at the same time, as shown in Fig. 2(b). The input power of the injected signal is -6.5 dBm. The oscillation frequencies are 9.998 and 16.083 GHz, and the powers are -0.2 and -0.3 dBm, respectively. The injection frequency is set at 6.085 GHz, which is exactly the frequency spacing of the two oscillation frequencies. The 6.085-GHz component in Fig. 2(b) is reflected from the electrical coupler and the MZM, owing to the impedance mismatch. The power of the two oscillation signals in Fig. 2(b) is about 4.1 dB smaller than that of the single frequency in Fig. 2(a), which is mainly caused by the loop gain reduction at two frequencies in one oscillation loop. It should be mentioned that the dual-frequency signal, which consists of two oscillation frequencies, can be separated into two frequencies using two narrowband filters. The frequency responses of the filters are schematically depicted in Fig. 2 with light-green and purple dashed lines.

Figure 3 displays the detailed frequency spectra of the two oscillation signals at the output of the DB-BPF in a 500-kHz span. The power values of the generated signals are normalized to 0 dBm for comparison. The S21 transmission responses of each passband of the DB-BPF are inserted as the insets in Figs. 3(a) and 3(b), respectively. The dashed curve in Fig. 3(a) shows the case when the injection signal is turned off, and

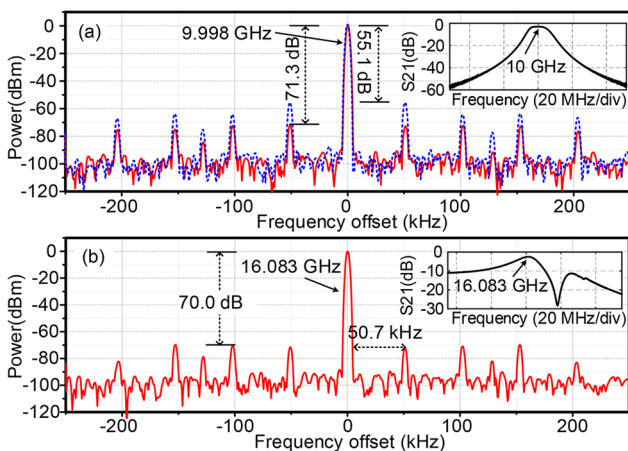


Fig. 3. Detailed electrical spectra at output of DB-BPF with span of 500 kHz. Insets: S21 responses of each passband of DB-BPF.

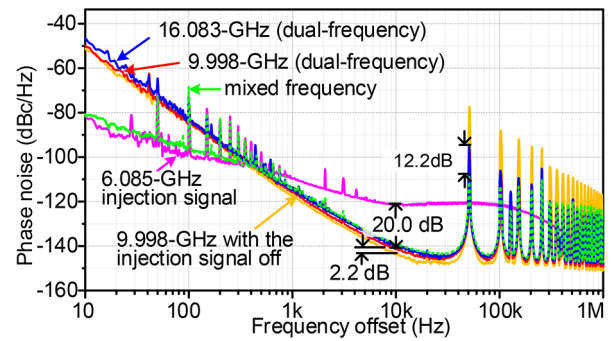


Fig. 4. Measured single-sideband PN spectra.

the sidemode suppression ratio (SMSR) is around 55.1 dB. The solid curve in Fig. 3(a) exhibits the electrical spectrum of the 9.998-GHz component with the injection signal turned on, the corresponding SMSR of which reaches 71.3 dB, showing a 16.2-dB improvement. The SMSR of the 16.083-GHz component is 70.0 dB in Fig. 3(b), and is much the same as that of the 9.998-GHz component. The SMSR improvement at both frequencies based on the proposed scheme is introduced by the injection locking mechanism [18]. The 50.7-kHz free spectrum range (FSR) of the generated signals shows that the loop length of the proposed OEO is around 4.03 km. It should be mentioned that the locking bandwidth and the SMSR of the oscillation frequencies will be affected by the injection power [19].

The measured single-sideband PN spectra of the RF signals in the proposed system are assessed and presented in Fig. 4. The orange solid curve shows the PN performance of the oscillating 9.998-GHz signal with the injection signal off, while the red and blue solid curves are those of the oscillating 9.998-GHz and 16.083-GHz frequencies with the injection signal on. Besides, the pink solid curve is the single-sideband PN spectrum of the 6.085-GHz injection signal. It can be easily observed that the PN curves of the two oscillation components of the dual-frequency signal coincide with each other well and reach around -140 dBc/Hz @ 10 kHz offset, which demonstrates that the proposed system successfully produces a dual-frequency signal with ultra-low PN. Compared with the case when the injection signal is switched off in the oscillation loop, the single-sideband PN of the 9.998-GHz frequency is increased by 2.2 dB with the injection signal on. The main reason is that the loop gain is shared by the two oscillation signals, which results in the signal-to-noise ratio (SNR) reduction for each frequency component. The generated dual-frequency signal has nearly 20-dB PN optimization to that of the injection signal at the frequency offset of 10 kHz, which means that the external injection frequency has little impact on the PN performance of the generated dual-frequency signal. To evaluate the coherence between the generated two oscillation frequencies, they are separated by two narrowband filters and then sent to a frequency mixer for frequency downconversion. The downconverted frequency has the same frequency as the injection signal. The PN spectrum (green dashed curve) of the downconverted frequency almost overlaps that of the injection signal at 10-Hz to 400-Hz frequency offset (pink solid curve), showing a 32-dB improvement on those of the two oscillation signals at the frequency offset of 10 Hz. The great improvement of the downconverted frequency in PN performance at low-frequency offsets indicates that the phase or frequency stability between the two frequency components

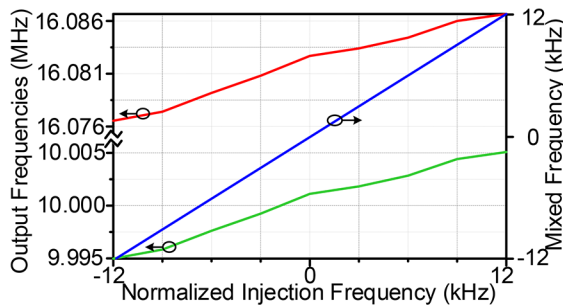


Fig. 5. Frequency tunability of proposed system.

is excellent, so they are highly coherent. It should be noted that the downconverted frequency signal also has a low PN of -139 dBc/Hz @ 10 kHz and a 12-dB SMSR improvement compared with the two oscillation signals, which makes it an attractive way to obtain low PN and high SMSR RF signals.

The frequency tunability of the proposed system is estimated by changing the injection frequency, and the results are shown in Fig. 5. The injection frequency is adjusted in a 24-kHz frequency span from 6.083054 to 6.083078 GHz, and the frequency tuning step of the injection signal is 1 kHz, which is shown as the horizontal axis in Fig. 5 with its frequency normalized. The key factor that decides the tuning range of the injection frequency is the locking bandwidth of the mutual injection locking effect, which is theoretically related to the injection power, the oscillation power, and the FSR [19]. As the injection frequency increases, the two oscillation frequencies at the output of the DB-BPF increase from 9.994981 to 10.005078 GHz (green curve) and from 16.078035 to 16.088156 GHz (red curve), respectively. The frequency tuning range of the two oscillation frequencies reaches around 10 MHz, which is mainly limited by the narrow passband of the DB-BPF. It should be noted that the rising trends of the two oscillation frequencies show a positive but not linear correlation to the injection frequency. The main reason is that the loop phase conditions, which determine the absolute oscillation frequencies of the OEO, are nonlinearly changed by the injection signal through the mutual injection locking mechanism. The frequency interval of the two oscillation frequencies is also measured by monitoring their downconverted frequency through a frequency mixer, which is shown as the blue curve in Fig. 5. It can be deduced from the blue curve that the downconverted frequency equals the injection frequency and exhibits a perfectly linear relationship with the injection frequency, which agrees well with the theory.

In conclusion, a novel approach for generating coherent dual-frequency signals is proposed based on an OEO. A DB-BPF is inserted in the OEO to select two different oscillation modes, and an external signal is injected into the OEO to stimulate mutual injection locking in the loop between the two oscillation signals. A dual-frequency signal of 9.998 GHz and 16.083 GHz is experimentally generated. Their PN values at 10-kHz fre-

quency offset reach -141.0 and -140.1 dBc/Hz, respectively. The PN curve of the 6.085-GHz downconverted frequency almost overlaps the injection signal at frequency offsets lower than 400 Hz and is 32 dB lower than the two oscillation signals at the 10-Hz frequency offset, which demonstrate the high phase coherence between the two oscillation frequencies. Moreover, the frequency tunability of the two oscillation signals is enabled by adjusting the injection frequency. The proposed method for phase-coherent dual-frequency signal generation may find applications in radar, communication, and precise measurement systems.

Funding. Key Technologies Research and Development Program (2022YFB2802700); Jiangsu Funding Program for Excellent Postdoctoral Talent (2022ZB237); National Natural Science Foundation of China (62001218, 62271249); Natural Science Foundation of Jiangsu Province (BK202000436).

Disclosures. The authors declare no conflicts of interest.

Data availability. Data underlying the results presented in this Letter are not publicly available at this time but may be obtained from the authors upon reasonable request.

REFERENCES

- W. Wiesbeck and L. Sit, in *2014 International Radar Conference* 1 (2014).
- F. Scotti, F. Laghezza, P. Ghelfi, and A. Bogoni, *IEEE Trans. Microwave Theory Tech.* **63**, 546 (2015).
- J. Vipul, T. Fred, L. Zhou, and H. Payam, *IEEE J. Solid-State Circuits* **44**, 3469 (2009).
- J. Kurdzo and R. Palmer, in *2011 IEEE Radar Conference* (2011), p. 231.
- S. Tejero, U. Siart, and J. Detlefsen, *Adv. Radio Sci.* **4**, 73 (2006).
- S. Pan and Y. Zhang, *J. Lightwave Technol.* **38**, 5450 (2020).
- A. Azad, F. Khan, and A. Caruso, *IEEE Trans. Plasma Sci.* **49**, 2183 (2021).
- T. Brandão, F. Scotti, and S. Cerqueira, *IET Radar, Sonar & Navigation* **13**, 505 (2019).
- H. Chen, B. Nakarmi, and S. Pan, *IEEE Photonics Technol. Lett.* **33**, 391 (2021).
- P. Zhou, H. Chen, N. Li, and S. Pan, *Opt. Lett.* **45**, 1342 (2020).
- J. Zhang, Y. Wang, X. Li, Z. Liu, and J. Wo, *Opt. Quantum Electron.* **53**, 407 (2021).
- Z. Xie, S. Li, H. Yan, and B. Zhou, *Opt. Express* **24**, 30282 (2016).
- P. Zhou, F. Zhang, and S. Pan, in *Conference on Lasers and Electro-Optics (CLEO)* (2015).
- B. Gao, F. Zhang, P. Zhou, and S. Pan, *IEEE Microw. Wireless Compon. Lett.* **27**, 192 (2017).
- F. Kong, W. Li, and J. Yao, *Opt. Lett.* **38**, 2611 (2013).
- E. C. Levy, M. Horowitz, and C. R. Menyuk, *J. Opt. Soc. Am. B* **26**, 148 (2009).
- F. He, R. Ribas, C. Lahurc, and M. Jézéquel, *Analog. Integr. Circ. Sig. Process.* **59**, 215 (2009).
- W. Zhou and G. Blasche, *IEEE Trans. Microwave Theory Tech.* **53**, 929 (2005).
- Z. Fang, J. Su, and Y. Lin, *Opt. Express* **29**, 4681 (2021).